- Determination of affinity of tetrahydrozoline enantiomers towards various cyclodextrins
- Affinity reversal observed based on structure of cyclodextrins
- Structure of guest-host complexes determined based on NMR spectroscopy
- Noncovalent forces in guest-host complexes computed
- Good correlations were observed between computed and experimentally observed affinity patterns

Separation of tetrahydrozoline enantiomers in capillary electrophoresis with cyclodextrin-type chiral selectors and investigation of chiral recognition mechanisms

Ann Gogolashvili[1], Ketevan Lomsadze[1,2], Lali Chankvetadze[1], Nino Takaishvili[1], Paola Peluso[3], Roberto Dallocchio[3], Antonio Salgado[4], Bezhan Chankvetadze[1*]

1) Institute of Physical and Analytical Chemistry, School of Exact and Natural Sciences, Tbilisi State University, Chavchavadze Ave 3, 0179 Tbilisi, Georgia
2) School of Science and Technology, The University of Georgia, 77a, M. Kostava str. 0171 Tbilisi, Georgia
3) Istituto di Chimica Biomolecolare ICB-CNR, Sede secondary a di Sassari, Traversa La Crucca 3, Regione Baldinca, Li Punti, 07100 Sassari, Italy
4) NMR Spectroscopy Centre (CERMN), CAI Químicas, Faculty of Pharmacy, University of Alcalá, E-28805 Alcalá de Henares, Madrid, Spain

*) Corresponding Author. E-mail: jpba_bezhan@yahoo.com

Abstract

The recognition power and affinity pattern of various cyclodextrins (CD) towards the enantiomers of tetrahydrozoline (THZ) were studied using capillary electrophoresis (CE). As expected, affinity of THZ enantiomers and selectivity of recognition towards CD derivatives was strongly dependent on the cavity size and substituent type and pattern on the CD rims. Not only were the affinity strength and selectivity of recognition affected by the size of the cavity and chemistry of the CDs but also the affinity pattern. Another interesting example of opposite affinity pattern of enantiomers towards α- and β-CD was observed here. In addition, opposite affinity pattern of THZ enantiomers was seen towards β-CD and its acetylated derivatives, while methylation of β-CD did not affect the affinity pattern of THZ enantiomers. In order to get more information about structural mechanisms of the multivariate dependences mentioned above, rotating frame Overhauser enhancement spectroscopy (ROESY) and computation techniques were used. Significant differences between the structure of THZ complexes with different CDs with both methods were encountered. Good correlations between experimentally determined and computed structure of complexes, as well as between computed complex stabilities and enantiomer migration order (EMO) in CE were observed.

Keywords:

Capillary electrophoresis; Nuclear magnetic resonance spectroscopy; Molecular Modeling, Tetrahydrozoline; Cyclodextrins; Chiral recognition mechanism.

1. Introduction

Capillary electrophoresis (CE) has been established as a particularly useful technique for analytical scale separation of enantiomers [1-4]. For this purpose, CE is widely used for problem solving in pharmaceutical [5], bioanalytical [6], environmental [7], food [7,8], and forensic analysis [7,9], as well as in analytical chemistry [7] and several other related fields. However, for abovementioned applications**,** CE has two strong rivals such as high-performance liquid chromatography (HPLC) [10-12] and supercritical fluid chromatography (SFC) [13]. Both of these techniques are competitive to CE for analytical scale separation of enantiomers. In addition, they offer possibilities for preparative, and even product scale separations [14-18]. For the latter**,** CE may have some potential [19-21] but is not commonly used. However, there is another application for what CE has an enormous strength and, in our opinion, currently there is no separation or non-separation technique that can compete with CE for this application. This field is investigation of noncovalent interactions. In the last decades, the interest toward noncovalent interactions have been growing more and more, and advancements in theoretical physical chemistry and computational techniques allowed for improving knowledge of noncovalent forces and developing new applications in several fields [22]. However, noncovalent interactions are weaker compared to covalent forces, and this inherent weakness makes their identification, profiling and application in solution more challenging compared to the solid state [23]. Instrumental separation methods based on noncovalent interactions, such as gas chromatography (GC), and in particular HPLC and SFC, can also be used to study these interactions [24-26]. In addition, non-separation methods, such as nuclear magnetic resonance (NMR) spectroscopy [27-29], optical spectroscopy [30,31], mass-spectrometry [32,33], atomic force microscopy and spectroscopy [34,35] and several other techniques are also suitable for this purpose. Moreover, computation methods provide useful tools for understanding possible structural mechanisms and computing forces involved

in inter- and intra-molecular noncovalent interactions [36-39]. Not only is a better understanding of noncovalent interactions important for a further advancement of chemistry but also for pharmacology, medicine, biology, physics and other related fields. CE offers unmatched detection sensitivity of weak intermolecular interactions in a liquid phase, this being an essential advantage for this purpose [40]. This study on the intermolecular interactions between the sympathomimetic drug tetrahydrozoline (THZ) and complexing agents cyclodextrins (CDs) discusses how CE based on its high sensitivity in sensing intermolecular interactions challenges other techniques (on their current level of development) for detecting and understanding the fine mechanisms of (enantioselective) intermolecular interactions.

2. Materials and Methods

2.1. Chemicals

Racemic tetrahydrozoline (tetryzoline) (2-(1,2,3,4-Tetrahydro-1-naphthalenyl)-4,5-dihydro-1H-imidazole, Fig. 1a), deuterium oxide (D_2O, 99 atom % D), sodium deuteroxide (NaOD, 40% w/w in D_2O, 99.5 atom % D), phosphoric acid (85%), deuterated phosphoric acid (85% w/w in D_2O, 98 atom % D), diethylamine, native α-, β- and γ-CDs, heptakis(2,6-di-O-methyl)-β-CD (H-2,6-DM-β-CD) and heptakis(2,3,6-tri-O-methyl)-β-CD (TM-β-CD) were purchased from Sigma-Aldrich (Saint-Louis, MO, USA). Heptakis(2,3-di-O-acetyl)-β-CD (HDA-β-CD) and heptakis(2,3-di-O-methyl)-β-CD (H-2,3-DM-β-CD) were prepared in our laboratory according to an earlier described methods [41]. Selectively sulfated β-CD derivatives, such as heptakis(6-O-sulfo)-β-CD (HS-β-CD), heptakis(2,3-di-O-methyl-6-O-sulfo)-β-CD (HDMS-β-CD), heptakis(2,3-di-O-acetyl-6-O-sulfo)-β-CD (HDAS-β-CD) and heptakis(2-O-methyl-3,6-di-O-sulfo)-β-CD (HMDS-β-CD) were kindly provided by Cyclolab (Budapest, Hungary). The schematic structures of CDs used in this study are shown in Fig.

1b. (+)- and (-)-THZ pure enantiomers were obtained as described in the subsection 2.2. Water was of Milli-Q quality (Millipore, Bedford, MA, USA). The background electrolyte (BGE) and sample solutions were filtered through Polypure polypropylene membrane filters (0.45 μm) from Alltech (Laarne, Belgium) before use.

2.2. Preparation of tetrahydrozoline enantiomers

The enantiomers of THZ were separated by HPLC using a Lux Cellulose 3 chiral column (4.6 mm× 250 mm with 5 μm particles, Phenomenex, Torrance, CA, USA) thermostated at 25°C. A mixture of n-hexane/propan-2-ol/diethylamine (80:20:0.1, v/v/v) was used as a mobile phase at a flow rate of 1.1 mL/min. A baseline separation of enantiomers with the resolution factor of 2.1 was obtained in 10 minutes with (-)-THZ eluting before the (+)-THZ (data not shown). Two fractions, corresponding to the (-)- and (+)-enantiomers of THZ, were separately collected. The purities of the collected fractions of (-)- and (+)-THZ were more than 99.5% enantiomer excess (ee) and 99.3% ee, respectively, based on HPLC. These enantiomerically "pure" fractions were used for spiking racemic THZ for determining EMO in CE.

It has been reported in earlier literature that THZ undergoes racemization via an imine–enamine tautomerism when enantioseparated on Chiralpak AD column in the mobile phase consisting of mixtures of ethanol, n-hexane and diethanolamine (DEA) [42]. This phenomenon was not observed on Lux Cellulose 3 column under the conditions mentioned in this subsection. However, we observed a racemization process under the analytical conditions used for NMR experiments as mentioned below.

2.3. Capillary electrophoresis

Enantioseparation of spiked THZ samples ((+)/(-) = 4/1) by CE was performed in 100 mM phosphoric acid buffer at pH 3.20 (adjusted with triethanolamine (TEA)) as background

electrolyte (BGE). Experimental conditions were as follows: uncoated fused-silica capillary, 50 μm I.D. and 375 μm O.D. and 31 (40) cm effective and total lengths, respectively. The samples were injected by pressure (50 mbar) for 2 s. The separation was performed under constant current mode (150 μA), the separation temperature was 20°C and the detection wavelength was set at 210 nm. Before each injection, the capillary was washed with 1 M NaOH for 2 min, then with BGE for another 2 min and finally, with BGE containing the chiral selector for another 2 min. At the end of each working day, the capillary was rinsed for 30 min with 0.1 M NaOH, 30 min with the BGE and 15 min with water. Capillary wash cycles were performed at a pressure of approximately 1 bar. The EMO was assigned by using the abovementioned spiking experiment.

2.4. NMR experiments

NMR spectra were recorded with a Bruker AVANCE 700 (Bruker Biospin, Fällanden, Switzerland), fitted with an inverse 5 mm QXI S4 700 probe head, z-gradient unit and variable temperature controller, and with a Varian Mercury Plus 300 (Varian Inc., Palo Alto, CA, USA), fitted with a 5 mm ATB $^{1}H,^{19}F/^{13}C,^{31}P$ probe head and z-gradient and variable temperature units. The concentration of the analytes in the NMR samples was about ca. 30-fold higher than in the CE experiments so that reproducible NMR spectra could be obtained. The solvent was 50 mM D_3PO_4 in D_2O, adjusted to an apparent pH 3 with sodium deuteroxide in D_2O (40% wt). Mixtures of enantiomerically pure THZ (1.8-3.9 mg in every case) with α-CD (15.1 mg), β-CD (10.0 mg) and HDAS-β-CD (10.0 mg) were each prepared by dissolving in 0.7 mL solvent. All samples were vortexed for 1 min and filtered through 0.45 μm polypropylene filters prior to data acquisition.

The ^{1}H 90° hard pulse width was optimized for each sample. The ^{1}H resonance frequency was 700.13 MHz and the ^{1}H spectral width was set to 14493 Hz. All NMR signals were assigned on the basis of COSY, TOCSY and HSQC data, when appropriate. For the 1D

ROESY experiments, the duration and the potency of the shaped pulse (Gaussian) were chosen according to the desired selectivity (180° pulse duration was arbitrarily set to 20, 40 or 60 ms, depending on more or less isolated spin systems). The duration of the low power pulse for mixing was 400 ms for all samples. The potency of this pulse was calculated according to that of a 90° pulse of 125 ms duration. The number of transients in each 1D ROESY experiment was set to 512. The ^{13}C NMR spectra of THZ were recorded at 75 MHz (^{1}H resonance frequency 300.16 MHz) with a ^{13}C spectral width of 15625 Hz (2500 scans each). All NMR experiments were run at 25 °C and every NMR spectrum was processed with the Mestre NOVA software (version 14.2.0, Mestrelab Research S. L., Santiago de Compostela, Spain).

2.5. Molecular modeling calculations

All calculations were performed by using the Spartan '10 Version 1.1.0 program (Wavefunction Inc., Irvine, CA, USA) [43]. The 3D structure of β-CD was released from Cambridge Structural Database (CSD) [44], entry AGAZOX [45]. HDAS- and HMDS-β-CD were built using CSD entry ICUFAN (heptakis(2,3,6-tri-O-acetyl) β-CD) as a template [46]. For HDAS-β-CD, the acetyl groups were removed from the O_{6n} positions ($1 \leq n \leq 7$) (see Supplementary data, Fig. S1 for the numbering of the CD skeleton) and replaced with sulfate substituents in all glucopyranose units. For HMDS-β-CD, all acetyl groups were removed and replaced with methyl and sulfate substituents at O_{2n} and O_{3n} / O_{6n} positions, respectively. The 3D structures of both THZ enantiomers (*S* and *R*) were generated from CSD entry SAXJIK (tetrahydrozoline hydrochloride) [47], and treated as doubly protonated, in accordance with the experimental pH = 3.2, thus bearing a positive charge unit after removing one of the chloride counteranions. All structures were prepared using the build function, model kits and tools provided by Spartan '10 for building and editing organic molecules. For each structure, geometry optimization was performed using the MMFF94s force field [48]. In addition,

geometry optimization and computation of electrostatic potential isosurfaces (V_S) (isovalue 0.002 au) (given in kcal/mol) of β-CD, HDAS- and HMDS-β-CD were also performed employing the Hartree-Fock (HF) method with STO-3G as basis set. The electrostatic potential in a point **r** (V(**r**)) is given by equation 1

$$V(\mathrm{r}) = \sum_A \frac{Z_A}{R_A - \mathbf{r}} - \int \frac{\rho(\mathbf{r})\mathrm{d}\mathbf{r}'}{|\mathbf{r}' - \mathbf{r}|} \quad (1)$$

where Z_A is the charge on nucleus A located at R_A, and ρ(**r**) is the electron density function.

The sign of V(**r**) is positive or negative if the effect of either the nuclei (first positive term) or that of electrons (second negative term) is the dominant one, respectively. The V_S maps were graphically generated through the graphical interface of Spartan '10 and, by convention, colours toward red or blue depict negative or positive potentials, respectively while colours in between (orange, yellow, green) refer to intermediate potential values. The complexes between the two THZ enantiomers and the three CDs were modelled by manually docking each analyte into the CD cavity. Then, each complex was submitted to a conformational systematic search using the Monte-Carlo algorithm, examining 1000 conformers spanning possible shapes open to a flexible molecule without consideration of energy, and keeping 10 low-energy conformers. On this basis, the lowest-energy conformations of all complexes ($92.6 \leq$ Boltzmann population (%) ≤ 100 in almost all cases) underwent geometry optimization using the MMFF94s force field. All geometry optimization procedures were performed in vacuum and water (SM5.4 model) [49]. Surface representations of THZ/CD complexes were graphically generated by using the Chimera 1.13.1 software [50]. The binding energy (E_{bindng}) between each THZ enantiomer and CD was calculated on the basis of the energies of the CD/THZ complex, CD and THZ enantiomer (eq. 2).

$$E_{binding} = E_{complex} - E_{THZ} - E_{CD} \quad (2)$$

Binding energy values are given in kcal/mol.

3. Results and Discussion

3.1. CE separation of THZ enantiomers

The separation parameters and observed migration order of THZ enantiomers are summarized in Table 1. Among native CDs α-CD exhibited the lowest recognition towards THZ enantiomers while its enantiorecognition pattern with THZ was opposite to that with β- and γ-CDs (Fig. 2a-c). This is another interesting example of enantiomer affinity reversal caused by the size of CD cavity [51-55]. Selective methylation of β-CD in positions 2 and 3 (H-2,3-DM-β-CD) or in positions 2 and 6 (H-2,6-DM-β-CD), as well as the permethylation in all available positions 2, 3 and 6 (TM-β-CD), did not significantly improve the resolving ability nor did it affect the affinity pattern of THZ enantiomers. In earlier studies the quite different separation ability and opposite affinity pattern towards TM-β-CD compared to β-CD was reported for the enantiomers of chlorpheniramine [56], brompheniramine [57], dimethindene [58] and verapamil [59] among other chiral compounds. Of the CD derivatives studied in this project the best enantiomer resolving ability was exhibited by HDAS-β-CD, even at the lowest concentration of all the CDs used in this study (Fig. 2d). The enantiomer migration order with HDAS-β-CD was opposite to that with native β-CD. Perhaps, acetylation of the wider secondary rim of β-CD is responsible for this affinity reversal since the affinity pattern of THZ enantiomers towards neutral analogue of HDAS-β-CD, namely heptakis (2,3-di-O-acetyl)-β-CD (HDA-β-CD), was the same as towards HDAS-β-CD with (+)-THZ reaching the detector first (Fig. 2e). The high enantiomer resolving ability of HDAS-β-CD, as well as the opposite affinity of enantiomers towards HDAS-β-CD and HDA-β-CD compared to β-CD are in good agreement with numerous earlier studies [31,60-64]. The affinity pattern of THZ enantiomers when using another sulfated, single component derivative of β-CD, namely HMDS-β-CD was also opposite to that seen with β-CD. Interestingly,

opposite enantiomer affinity patterns between β-CD and HMDS-β-CD was also observed for many other analytes, as reported in our earlier studies [65-67].

Thus, CE experiment also on THZ enantiomers confirmed that HDA-β-CD, HDAS-β-CD and HMDS-β-CD recognize the enantiomers based on an apparently quite different mechanism compared to the native β-CD. Further studies using NMR spectroscopy were performed on THZ complexes with the three CDs, namely α-CD, β-CD and HDAS-β-CD.

3.2. NMR study of THZ / CD complexes

All ^{1}H NMR signal assignments are shown in Table 2. As already mentioned and unlike in our HPLC analyses (-)-THZ easily racemized in the presence of all the studied CDs under the conditions used for NMR experiments. The racemization was especially clearly visible in the ^{13}C-NMR spectra (Fig. 3). Although the guest-CD molar ratios were not exactly the same in each sample these spectra also indicate that HDAS-β-CD differentiates the enantiomers of THZ better than β- and, especially α-CD. This is supported by the increased number of ^{13}C-NMR signals due to nonequivalence of complexation induced chemical shits for enantiomers, as well as based on the values of chemical shift differences between the diastereotopic signals (Fig. 3). This observation in NMR spectroscopy correlates well with the observations in CE.

3.2.1. (-)-THZ / α-CD complex

The ^{1}H-NMR spectrum of the mixture of (-)-THZ and α-CD was very crowded with some critical overlapping between the THZ and α-CD protons (Fig. 4). Thus, the discussion regarding the possible structure of the complex was mostly based on the shape (multiplicity) and intensity of NOE responses. Some of the irradiation experiments were quite informative. Clear NOE response was observed on the H-3 and H-5 hydrogens of α-CD (Fig. 4) upon

irradiation at the partially overlapped H-5’ and H-6’ and also the H-7’ protons of THZ. When the H-8’ hydrogens of THZ were irradiated a strong NOE response was observed on the H-3 protons of α-CD while the effect on the H-5 hydrogen atoms of α-CD was almost negligible (Fig. 4). Irradiation of H-1’ protons of THZ resulted in NOE interaction only with the H-3 hydrogens of α-CD. No reliable intermolecular NOE response was observed when THZ H-2’, H-3’ and H-4’ protons were excited. It has to be mentioned that the H-3 of α-CD is partially overlapped with the imidazoline protons of THZ and with α-CD’s H-6. Thus, one can suspect that the NOE responses upon irradiation on THZ positions considered above may be the result of TOCSY correlations (which is an intramolecular not an intermolecular effect). However, the shape (clearly a triplet) and the coupling constant (ca. 10 Hz) seen in the ROESY experiment are compatible with an intermolecular NOE interaction involving the H-3 protons of α-CD, as mentioned above. Based on these results a structure of the THZ / α-CD complex was derived as shown in Fig. 5a. This structure was confirmed based on the irradiation of protons of α-CD and observing the NOE interactions on THZ protons (data not shown).

3.2.2. (-)-THZ / β-CD complex

The ^{1}H NMR spectrum of the mixture of (-)-THZ and β-CD looked better resolved than that of the THZ and α-CD mixture (Fig. 6). Intermolecular NOEs involving the internal H-3 and H-5 hydrogens of β-CD point at an inclusion complex. These NOE interactions look more intense with the H-3 protons compared to H-5 protons of β-CD. Irradiation at H-3 protons of β-CD gives NOE response mainly with the aromatic H-8’ and aliphatic H-4’ of THZ, but not with imidazoline nor the aliphatic H-1’, H-2’ and H-3’ protons of THZ. This indicates at an inclusion complex in which the aromatic moiety of THZ enters the β-CD cavity through the wider opening, while the imidazoline ring remains out of the cavity. Thus, the most likely structure of the (-)-THZ / β-CD complex in solution looks as shown in Fig. 5b.

Interestingly, inclusion of the analyte molecule into the CD cavity seems to be somewhat deeper compared to α-CD.

3.2.3. (-)-THZ / HDAS-β-CD complex

The ^{1}H NMR spectrum of the mixture of (-)-THZ and HDAS-β-CD was the best resolved among all THZ-CD mixtures used for NMR experiment in this study (Fig. 7). We found only two sites in the ^{1}H spectrum with some degree of overlapping,-namely one of the two H-6 protons of HDAS-β-CD overlapped with the H-1' protons of the tetrahydronaphthyl moiety of THZ, and the H-4 and H-5 hydrogens of HDAS-β-CD which completely overlapped to each other. Since there were two signals assignable for H-6 protons of HDAS-β-CD the one involved in abovementioned overlapping was not considered for diagnostic purposes. In addition, it is less likely that the H-4 external hydrogens get directly involved in intermolecular interactions with an analyte, especially when inclusion complexes are formed. Thus, one may assume that intermolecular NOE responses observed on overlapping signals of H-4 and H-5 protons of HDAS-β-CD at 4.11 ppm are solely due to HDAS-β-CD H-5 hydrogens.

Upon irradiation of H-5' and H-7' protons of THZ significantly stronger response was observed on the abovementioned overlapped signals of H-4 and H-5 protons of HDAS-β-CD compared to that on H-3 protons. This difference in the intensity of the NOE response was also the case yet less expressed when the H-6' protons of THZ were irradiated. The NOE response on HDAS-β-CD hydrogens was weak upon irradiation at the H-8' protons of THZ but among all the HDAS-β-CD hydrogens the overlapped H-4 and H-5 protons of HDAS-β-CD gave the strongest NOE. There was no significant (reliable) NOE response observed on HDAS-β-CD protons upon irradiation of any other proton of THZ. Thus, based on these

290 results the structure of the complex as shown in Fig. 5c could be proposed. This structure was
291 confirmed by irradiation at some HDAS-β-CD positions (data not shown).
292 There was no major difference between the NMR-derived structures of complexes of
293 THZ with α- and β-CD, although the affinity pattern of THZ enantiomers towards these two
294 CDs were opposite to each other. On the other hand, the structure of THZ complex with
295 HDAS β-CD is very different from the structure of the same guest molecule with α- and β-
296 CDs.
297
298 *3.3. Molecular modelling*
299 *3.3.1. Modelling of native and sulfated β-CDs*
300 In the native β-CD the cyclic oligosaccharide is linked by seven α-(1,4) glucose units which
301 are all in the $^4C_1$ chair conformation (Supplementary data, Fig. S1) [68]. The cavity shape of β-
302 CD is relatively rounded. In order to monitor the extent to which the cavity shape of the β-CD
303 adapts after calculations Chao and co-authors used $\Delta R_{l\text{-}s}$ which is defined as the calculated
304 difference between the longest and the shortest O···O distances from the seven pairs of
305 opposing glycosidic oxygen atoms of the CD (Supplementary data, Fig. S1) [68]. A small value
306 of $\Delta R_{l\text{-}s}$ indicates that the cavity shape is rounded, whereas a high value reveals an elliptic
307 distorted cavity. On this basis, the calculated structure of β-CD with MMFF94s force field and
308 the HF/STO-3G method proved to be consistent with the crystal structure of the CD (CSD,
309 entry AGAZOX) with $\Delta R_{l\text{-}s}$ of 0.150, 0.011 and 0.172, respectively (Supplementary data, Table
310 S1 and Fig. S2). Otherwise, persubstitution of both primary and secondary hydroxyl oxygen
311 atoms tend to increase CD flexibility, due to the absence of intramolecular hydrogen bonds (H-
312 bonds) sustaining the roundness of the ring. In this case, the macrocycle may become elliptically
313 distorted. For instance, this situation has been observed for peracetylated β-CD, the acetyl side
314 chains interfering with the ability of the peracetylated system to form inclusion complex [46].

315 In accord with these observations, distorted rings were observed in calculated structures of both
316 HDAS- and HMDS-β-CD (Supplementary data, Fig. S3). Coherently, flexibility and ellipticity
317 of the ring skeleton, measured as $\Delta R_{l\text{-}s}$ increases following the order β-CD < HMDS-β-CD <
318 HDAS-β-CD (Supplementary data, Tables S2-S4). Thus, the primary hydroxyl group region
319 appeared wider (Supplementary data, Fig. S4).

320 Given that, with the aim of exploring comparatively the impact of CD shape, which is given
321 by the sum of geometry and electron distribution, on the enantioseparation results, V_S of β-CD,
322 HDAS- and HMDS-β-CD were calculated and compared. Indeed, V_S proved to be useful to
323 assess electronic properties and interaction capability of specific atoms and sites [36]. In Figure
324 8, the V_S of the three CDs are compared with the same V range, defined by the limits of the
325 most positive potential calculated for the β-CD (39.0 kcal/mol) and the most negative potential
326 calculated for the HMDS-β-CD (-556.1 kcal/mol).

327 On one hand, the comparison of the overall electronic distribution showed that the electron
328 charge density increases in the order β-CD < HDAS-β-CD < HMDS-β-CD. On the other hand,
329 the surface area of the CDs ($Å^2$) increases following the order β-CD (924.22) < HMDS-β-CD
330 (1701.17) < HDAS-β-CD (1763.02). In this regard, it is worth noting that for HDAS-β-CD a
331 bowl-shaped structure was calculated with an extended surface exposed. In particular, the
332 secondary rim of HDAS-β-CD is completely closed by the self-inclusion of the 2,3-di-O-acetyl
333 groups, as reported for the heptakis(2,3,6-tri-O-acetyl)-β-CD [46].

334 Finally, the evaluation of the electron charge density distribution in each CDs showed other
335 differences between the three CDs (Supplementary data, Fig. S4). In Fig. S4,a-c the three CDs
336 are viewed from the secondary hydroxyl rim, whereas in Fig. S4,d-f the views from the primary
337 hydroxyl rim are depicted. In the β-CD, the secondary rim (Fig. S4a) shows more electron
338 charge density compared to the primary rim (Fig. S4d). The opposite situation occurs for the
339 HMDS-β-CD (Fig. S4c vs S4f) and even more for the bowl-shaped HDAS-β-CD (Fig. S4b,e).
340

3.3.2. Modelling of THZ / CD complexes

After conformational systematic search using the Monte-Carlo algorithm, the calculated lowest-energy conformations showed Boltzmann population (BD%) ranging from 92.6 to 100% in almost all cases. Only in the case of the complex (*S*)-THZ / HMDS-β-CD two low-energy conformers were found with the (*S*)-enantiomer located at the secondary (60.8%) and the primary rim (39.2%), respectively. In Table 3 calculated $E_{binding}$, $\Delta E_{binding}$, and calculated and experimental EMO are summarized.

A surface-based representation of the calculated complexes are depicted in Figure 9.

The energy calculations of the CD complexes were performed with and without consideration of aqueous medium. It is interesting to note that the calculated affinity pattern of THZ enantiomers towards β-CD on the one side, and HMDS-β-CD and HDAS-β-CD, on the other one, was opposite. This is in a good agreement with EMO reversal between the same CDs observed in CE. Absolute stereochemical configuration of (+)- and (-)-THZ is not known at least to the best of our knowledge. Based on CE experiments of this study and computed affinity pattern of (S)- and (R)-THZ towards the CDs one can assume that (+)-THZ has the (R) and (-)-THZ the (S) absolute stereochemical configuration. This is in a good agreement with the absolute stereochemical configuration of structural analogues of THZ described in the literature [69]. Thus, as this study shows CE in combination with molecular modelling techniques can be used for a tentative assignment of absolute stereochemical configuration of chiral compounds. In the complexes of both enantiomers with β-CD, an HB between the imidazole proton and the 3-OH was observed with distances of 1.680 and 1.625 Å for (*S*)- and (*R*)-enantiomers, respectively. Shorter H-bond distances ranging from 1.515 to 1.577 Å were found for both HMDS-β-CD and HDAS-β-CD complexes, respectively, involving the imidazole protons and the charged sulfate regions.

It has to be noticed that although the computed energy of complexes correlates well with the affinity pattern of THZ enantiomers in CE, the energy differences between the complexes

of two enantiomers with CDs do not correlate that well with the recognition power observed in CE experiment. Thus, for instance, from the results reported in Table 1 it is obvious that HDAS-β-CD is much better chiral selector compared to native β-CD or HMDS-β-CD for THZ enantiomers. Molecular modelling data, especially in aqueous medium, do not indicate any preference of HDAS-β-CD over two other CDs from the viewpoint of recognition selectivity (Table 3).

4. Conclusions

The affinity patterns of THZ enantiomers towards native α-, β- and γ-CD and single component neutral and sulfated derivatives of β-CD were studied by CE. Changes on these patterns were observed depending on the cavity size of the CD, and on the presence and location of substituents in the case of β-CD derivatives. Based on CE experiments anionic HDAS-β-CD appeared to be the best chiral selector providing the highest separation factor of enantiomers at the lowest concentration in the background electrolyte. In order to gain some insight regarding the structural reasons of the affinity reversal of THZ enantiomers towards α-CD and β-CD, as well as between β-CD and HDAS-β-CD, the structures of the complexes of THZ enantiomers with these 3 CDs in the solution were studied based on 1D ROESY experiments. Only minor structural differences were observed between the complexes of THZ with both native CDs whereas the structure of the THZ / HDAS-β-CD complex was very different from those with native CDs. Molecular modeling studies performed on β-CD, HDAS-β-CD and HMDS-β-CD indicated that self-inclusion of the acetyl moieties into the cavity of HDAS-β-CD through its secondary rim hinders the inclusion of the analyte by the same side of the CD. This may explain why the inclusion of aromatic moiety of THZ into the cavity of HDAS-β-CD occurs through the narrower primary rim.

Acknowledgements

393 This project was supported financially in part by the Shota Rustaveli National Science
394 Foundation (RNSF) of Georgia (Project No. 217642). We also thank Cyclolab Ltd (Budapest,
395 Hungary) for providing free samples of some cyclodextrins used in this study.
396

References

[1] C. Fanali, S. Fanali, Chiral separations using miniaturized techniques: State of the art and perspectives, Isr. J. Chem. 56 (2016) 958-967. DOI: 10.1002/ijch.201600061.

[2] P. Jáč, G.K.E. Scriba, Recent advances in electrodriven enantioseparations, J. Sep. Sci. 36 (2013) (1) 52-74. DOI: 10.1002/jssc.201200836.

[3] V. Kašička, Recent developments in capillary and microchip electroseparations of peptides, Electrophoresis 41 (2020) 10-35. DOI: 10.1002/elps.201900269

[4] S. Fanali, B. Chankvetadze, Some thoughts about enantioseparations in capillary electrophoresis, Electrophoresis 40 (2019) 2420-2437. DOI: 10.1002/elps.201900144

[5] S. Krait, M. Konjaria, G.K.E. Scriba, Advances of capillary electrophoresis enantioseparations in pharmaceutical analysis, Electrophoresis 42 (2021) in press. DOI: 10.1002/elps.202000359

[6] J. Caslavska, W. Thormann, Bioanalysis of drugs and their metabolites by chiral electromigration techniques, Electrophoresis 42 (2021) in press. DOI?

[7] S. Bernardo-Bermejo, E. Sánchez-López, M. Castro-Puyana, M.L. Marina, Chiral capillary electrophoresis, Trends Anal. Chem. 124 (2020) 115807. DOI: 10.1016/j.trac.2020.115807.

[8] M. Herrero, C. Simó, V. García-Cañas, S. Fanali, A. Cifuentes, Chiral capillary electrophoresis in food analysis, Electrophoresis 31 (2010) 2106-2114. DOI: 10.1002/elps.200900770.

[9] N. Anastos, N.W. Barnett, S.W. Lewis, Capillary electrophoresis for forensic drug analysis: A review, Talanta 67 (2005) 269-279. DOI: 10.1016/j.talanta.2005.03.038.

[10] G.K.E. Scriba, Chiral recognition in separation sciences. Part I: Polysaccharide and cyclodextrin selectors, TrAC - Trends Anal. Chem. 120 (2019) 115639. DOI: 10.1016/j.trac.2019.115639

[11] J. Shen, Y. Okamoto, Efficient separation of enantiomers using stereoregular chiral polymers, Chem. Rev. 116 (2016) 1094-1138. DOI: 10.1021/acs.chemrev.5b00317

[12] B. Chankvetadze, Recent trends in preparation, investigation and application of polysaccharide-based chiral stationary phases for separation of enantiomers in high-performance liquid chromatography, Trends Anal. Chem. 122 (2020) 115709 (13pp). DOI: 10.1016/j.trac.2019.115709

[13] C. West, Recent trends in chiral supercritical fluid chromatography, Trends Anal. Chem. 120 (2019) 115648. DOI: 10.1016/j.trac.2019.115648.

[14] D. Speybrouck, E. Lipka, Preparative supercritical fluid chromatography: A powerful tool for chiral separations, J. Chromatogr. 1467 (2016) 33-55. DOI: 10.1016/j.chroma.2016.07.050.

[15] D. Speybrouck, M. Howsam, E. Lipka, Recent developments in preparative-scale supercritical fluid- and liquid chromatography for chiral separations, TrAC - Trends Anal. Chem. 133 (2020) 116090. DOI: 10.1016/j.trac.2020.116090.

[16] M. Gumustas, S. A. Ozkan, B. Chankvetadze, Analytical and preparative separation of enantiomers of chiral drugs by chromatography and related methods, Curr. Med. Chem., 25(33) (2018) 4152-4188. DOI: 10.2174/0929867325666180129094955.

[17] H. Leek, S. Andersson, Preparative scale resolution of enantiomers enables accelerated drug discovery and development, Molecules 22 (2017) 158. DOI: 10.3390/molecules22010158.

[18] M. Boberg, A.C. Jonson, H. Leek, R. Jansson-Löfmark, M. Ashton, Chiral chromatographic isolation on milligram scale of the human african trypanosomiasis treatment d - and l -Eflornithine. ACS Omega 5 (2020) 23885-23891. DOI: 10.1021/acsomega.0c03121.

[19] B. Chankvetadze, N. Burjanadze, D. Bergenthal, G. Blaschke, Potential of flow-counterbalanced capillary electrophoresis for analytical and micropreparative

separations, Electrophoresis, 20 (1999) 2680-2685. (PDF). DOI: 10.1002/(sici)1522-2683(19990901)20:13<2680::aid-elps2680>3.0.co;2-%23.

[20] I. Spanik, P. Lim, G. Vigh, Use of full-column imaging capillary isoelectric focusing for the rapid determination of the operating conditions in the preparative-scale continuous free-flow isoelectric focusing separation of enantiomers, J. Chromatogr. A 960 (2002) 241-246. DOI: 10.1016/S0021-9673(02)00504-6.

[21] B. Thome, C.F. Ivory, Continuous fractionation of enantiomer pairs in free solution using an electrophoretic analog of simulated moving bed chromatography, J. Chromatogr. A 953 (2002) 263-277. DOI: 10.1016/S0021-9673(02)00097-3.

[22] I. Alkorta, J. Elguero, A. Frontera, Not only hydrogen bonds: other noncovalent interactions, Crystals 10 (2020) 180. DOI: 10.3390/cryst10030180.

[23] H.–J. Schneider, Quantification of noncovalent interactions – promises and problems, New J. Chem. 43 (2019) 15498-15512. DOI: 10.1039/c9nj03325d.

[24] M. Boumahraz, V. Ya. Davydov, M.P. Elizalde-González, A. V. Kiselev Intermolecular interactions in liquid adsorption chromatography, Chromatographia 17 (1983) 143-148. DOI: 10.1007/BF02271037.

[25] T. Cserhati, K. Valko, Chromatographic Determination of Molecular Interactions. Applications in Biochemistry, Chemistry, and Biophysics, CRC Press (1993) 392 pp. ISBN 9780849344374.

[26] T. Hanai, In silico modeling study on molecular interactions in reversed-phase liquid chromatography, J. Chromatogr. Sci. 53 (2015) 1084–1091. DOI: 10.1093/chromsci/bmu170

[27] G. Otting, K. Wüthrich, Heteronuclear filters in two-dimensional [1H, 1H]-NMR spectroscopy: combined use with isotope labelling for studies of macromolecular

conformation and intermolecular interactions, Quarterly Reviews of Biophysics 23 (1990) 39-96. DOI: 10.1017/S0033583500005412.

[28] M. Pellecchia, Solution nuclear magnetic resonance spectroscopy techniques for probing intermolecular interactions, Chemistry & Biology 12 (2005) 961-971. DOI: 10.1016/j.chembiol.2005.08.013.

[29] A. Salgado, B. Chankvetadze, Applications of nuclear magnetic resonance spectroscopy for the understanding of enantiomer separation mechanisms in capillary electrophoresis, J. Chromatogr. A 1467 (2016) 95-144. DOI: 10.1016/j.chroma.2016.08.060.

[30] J. Sadlej, J.Cz. Dobrowolski, J.E. Rode, VCD spectroscopy as a novel probe for chirality transfer in molecular interactions, Chem. Soc. Rev. 39 (2010) 1478-1488. DOI: 10.1039/b915178h.

[31] C. Merten, Vibrational optical activity as probe for intermolecular interactions, Phys. Chem. Chem. Phys. 19 (2017) 18803-18812. DOI: 10.1039/c7cp02544k.

[32] T. Wyttenbach, M.T. Bowers, Intermolecular interactions in biomolecular systems examined by mass spectrometry, Ann. Rev. Phys. Chem. 58 (2007) 511-533. DOI: 10.1146/annurev.physchem.58.032806.104515

[33] G. Chen, M. Fan, Y. Liu, B. Sun, M. Liu, J. Wu, N. Li, M. Guo, Advances in MS based strategies for probing ligand-target interactions: Focus on soft ionization mass spectrometric techniques, Front. Chem. 7 (2019) 703. DOI: 10.3389/fchem.2019.00703.

[34] A. Berquand, M.-P. Mingeot-Leclercq, Y.F. Dufrêne, Real-time imaging of drug–membrane interactions by atomic force microscopy, Biochimica et Biophysica Acta (BBA) – Biomembranes, 1664 (2004) 198-205.-DOI: 10.1016/j.bbamem.2004.05.010

[35] A.R. Bizzarri, S. Cannistraro, The application of atomic force spectroscopy to the study of biological complexes undergoing a biorecognition process, Chem. Soc. Rev. 39 (2010) 734-749. DOI: 10.1039/b811426a.

[36] P. Peluso, V. Mamane, R. Dallocchio, A. Dessi, S. Cossu, Noncovalent interactions in high-performance liquid chromatography enantioseparations on polysaccharide-based chiral selectors, J. Chromatogr. A 1623 (2020)461202. DOI: 10.1016/j.chroma.2020.461202

[37] R. Sardella, E. Camaioni, A. Macchiarulo, A. Gioiello, M. Marinozzi, A. Carotti, Computational studies in enantioselective liquid chromatography: Forty years of evolution in docking- and molecular dynamics-based simulations, TrAC - Trends Anal. Chem. 122 (2020) 115703. DOI: 10.1016/j.trac.2019.115703.

[38] R. Sardella, F. Ianni, L. Cossignani, G. Aldini, A. Carotti, Binding modes identification through molecular dynamic simulations: A case study with carnosine enantiomers and the Teicoplanin A2-2-based chiral stationary phase, J. Sep. Sci. 43 (2020) 1728-1736. DOI: 10.1002/jssc.202000092.

[39] P. Peluso, B. Chankvetadze, The molecular bases of chiral recognition in 2-(benzylsulfinyl)benzamide enantioseparation, Anal. Chim. Acta, 1141 (2021) 194-205. DOI: 10.1016/j.aca.2020.10.050.

[40] B. Chankvetadze, Contemporary theory of enantioseparations in capillary electrophoresis, J. Chromatogr. A, 1567 (2018) 2-25. DOI: 10.1016/j.chroma.2018.07.041.

[41] K. Takeo, H. Mitoh, K. Uemura, Selective chemical modification of cyclomalto-oligosaccharides via tert-butyldimethylsilylation, Carbohydr. Res. 187 (1989) 203–221. DOI: 10.1016/0008-6215(89)80004-7

[42] S. Caccamese, G. Principato, Resolution of the enantiomers of tetrahydrozoline by chiral HPLC. The racemization of the enantiomers via an imine–enamine tautomerism, Tetrahedron: Asymmetry 9 (1998) 2939–2945. DOI: 10.1016/S0957-4166(98)00300-0.

[43] Y. Shao, L.F. Molnar, Y. Jung, J. Kussmann, C. Ochsenfeld, S.T. Brown, A.T.B. Gilbert, L.V. Slipchenko, S.V. Levchenko, D.P. O'Neil, R.A. Di Stasio Jr, R.C. Lochan, T. Wang, G.J.O. Beran, N.A. Besley, J.M. Herbert, C.Y. Lin, T. VanVoorhis, S.H. Chien, A. Sodt, R.P. Steele, V.A. Rassolov, P.E. Maslen, P.P. Korambath, R.D. Adamson, B. Austin, J. Baker, E.F.C. Byrd, H. Dachsel, R.J. Doerksen, A. Dreuw, B.D. Dunietz, A.D. Dutoi, T.R. Furlani, S.R. Gwaltney, A. Heyden, S. Hirata, C.-P. Hsu, G. Kedziora, R.Z. Khalliulin, P. Klunzinger, A.M. Lee, M.S. Lee, W.Z. Liang, I. Lotan, N. Nair, B. Peters, E.I. Proynov, P.A. Pieniazek,Y.M. Rhee, J. Ritchie, E. Rosta, C.D. Sherrill, A.C. Simmonett, J.E. Subotnik, H.L. Woodcock III, W. Zhang, A.T. Bell, A.K. Chakraborty, D.M. Chipman, F.J. Keil, A.Warshel, W.J. Hehre, H.F. Schaefer, J. Kong, A.I. Krylov, P.M.W. Gill, M. Head-Gordon, Advances in methods and algorithms in a modern quantum chemistry program package, Phys. Chem. Chem. Phys. 8 (2006) 3172–3191. DOI: 10.1039/b517914a.

[44] I.R. Thomas, I.J. Bruno, J.C. Cole, C.F. Macrae, E. Pidcock, P.A. Wood, WebCSD: the online portal to the Cambridge structural database, J. Appl. Cryst. 43 (2010) 362–366. DOI: 10.1107/S0021889810000452.

[45] J.M. Alexander, J.L. Clark, T.J. Brett, J.J. Stezowski, Chiral discrimination in cyclodextrin complexes of amino acid derivatives: β-cyclodextrin/N-acetyl-L-phenylalanine and N-acetyl-D-phenylalanine complexes, Proc. Natl. Acad. Sci. U.S.A. 99 (2002) 5115–5120. DOI: 10.1073/pnas.072647599.

[46] M. Añibarro, K. Gessler, I. Usón, G.M. Sheldrick, K. Harata, K. Uekama, F. Hirayama, Y. Abe, W. Saenger, Effect of peracylation of β-cyclodextrin on the molecular structure and on the formation of inclusion complexes: an X-ray study, J. Am. Chem. Soc. 123 (2001) 11854–11862. DOI: 10.1021/ja010696b.

[47] S. Ghose, J.K. Dattagupta, Structure of tetrahydrozoline hydrochloride, Acta Cryst. C45 (1989) 1522–1524. DOI: 10.1107/S0108270189001447

[48] T.A. Halgren, MMFF VI. MMFF94s option for energy minimization studies, J. Comput. Chem. 20 (1999) 720–729. DOI: 10.1002/(SICI)1096-987X(199905)20:7<720::AID-JCC7>3.0.CO;2-X.

[49] C.C. Chambers, G.D. Hawkins, C.J. Cramer, D.G. Truhlar, Model for aqueous solvation based on class IV atomic charges and first solvation shell effects, J. Phys. Chem. 100 (1996) 16385–16398. DOI: 10.1021/jp9610776.

[50] E.F. Pettersen, T.D. Goddard, C.C. Huang, G.S. Couch, D.M. Greenblatt, E.C. Meng, T.E. Ferrin, UCSF Chimera - a visualization system for exploratory research and analysis. J. Comput. Chem. 25 (2004) 1605–1612. DOI: 10.1002/jcc.20084.

[51] B. Chankvetadze, M. Fillet, N. Burjanadze, D. Bergenthal, C. Bergander, H. Luftmann, J. Crommen, G. Blaschke, Enantioseparation of aminoglutethimide with cyclodextrins in capillary electrophoresis and studies of selector-selectand interactions using NMR spectroscopy and electrospray ionization mass spectrometry, Enantiomer, 5 (2000) 313-322. PubMed ID: 11126872. ISSN: 10242430.

[52] E. Domínguez Vega, K. Lomsadze, L. Chankvetadze, A. Salgado, G. Scriba, E. Calvo, J. A. López, A. L. Crego, M. L. Marina and B. Chankvetadze, Separation of enantiomers of ephedrine by capillary electrophoresis using cyclodextrins as chiral selectors: Comparative CE and NMR studies, Electrophoresis, 2011, 32, 2640-2647. DOI: 10.1002/elps.201100015.

[53] K. Lomsadze, E. Domínguez Vega, A. Salgado, A. L. Crego, G. K.E. Scriba, M. L. Marina, B. Chankvetadze, Separation of enantiomers of norephedrine by capillary electrophoresis using cyclodextrins as chiral selectors: Comparative CE and NMR studies, Electrophoresis, 2012, 33, 1637-1647. DOI: 10.1002/elps.201200062.

[54] M.-L. Konjaria, G.K.E. Scriba, Enantioseparation of analogs of the dipeptide alanyl-phenylalanine by capillary electrophoresis using neutral cyclodextrins as chiral selectors, J. Chromatogr. A 1623 (2020), Article number 461158. DOI: 10.1016/j.chroma.2020.461158.

[55] A. Gogolashvili, L. Chankvetadze, N. Takaishvili, A. Salgado, B. Chankvetadze, Separation of terbutaline enantiomers in capillary electrophoresis with neutral cyclodextrin-type chiral selectors and investigation of the structure of selector-selectand complexes using nuclear magnetic resonance spectroscopy, Electrophoresis, 41 (2020) 1023-1030. DOI: 10.1002/elps.202000010.

[56] B. Chankvetadze, G. Pintore, N. Burjanadze, D. Bergenthal, D. Strickmann, R. Cerri, G. Blaschke, Capillary electrophoresis, nuclear magnetic resonance and mass-spectrometric studies of opposite chiral recognition of chlorpheniramine enantiomers with various cyclodextrins, Elecrophoresis, 19 (1998) 2101-2108. DOI: 10.1002/elps.1150191210.

[57] B. Chankvetadze, N. Burjanadze, G. Pintore, D. Bergenthal, K. Bergander, C. Mühlenbrock, J. Breitkreutz, G. Blaschke, Separation of brompheniramine enantiomers by capillary electrophoresis and study of chiral recognition mechanisms of cyclodextrins using NMR-spectroscopy, UV-spectrometry, ESI-MS and x-ray crystallography, J. Chromatogr. A, 875 (2000) 471-484. DOI: 10.1016/S0021-9673(00)00153-9.

[58] B. Chankvetadze, G. Pintore, N. Burjanadze, D. Bergenthal, K. Bergander, J. Breitkreutz, C. Mühlenbrock, G. Blaschke, Mechanistic study of opposite migration order of dimethindene enantiomers in capillary electrophoresis in the presence of native β-CD and heptakis-(2,3,6-tri-O-methyl)-β-CD. J. Chromatogr. A, 875 (2000) 455-469. DOI: 10.1016/S0021-9673(00)00146-1.

[59] B. Chankvetadze, N. Burjanadze, G. Pintore, D. Strickmann, D. Bergenthal, G. Blaschke, Chiral recognition of verapamil by cyclodextrins studied with capillary electrophoresis, NMR- and mass-spectrometry, Chirality 11 (1999) 635-644. DOI: 10.1002/(SICI)1520-636X(1999)11:8<635:AID-CHIR5>3.0.CO;2-D.

[60] M. Wedig, U. Holzgrabe, Resolution of ephedrine derivatives by means of neutral and sulfated heptakis(2,3-di-O-acetyl)β-cyclodextrins using capillary electrophoresis and nuclear magnetic resonance spectroscopy, Electrophoresis 20 (1999) 2698-2704. DOI: 10.1002/(SICI)1522-2683(19990901)20:13<2698::AID-ELPS2698>3.0.CO;2-N

[61] C. Hellriegel, H. Händel, M. Wedig, S. Steinhauer, F. Sörgel, K. Albert, U. Holzgrabe, Study on the chiral recognition of the enantiomers of ephedrine derivatives with neutral and sulfated heptakis(2,3-O-diacetyl)-β-cyclodextrins using capillary electrophoresis, UV, nuclear magnetic resonance spectroscopy and mass spectrometry, J. Chromatogr. A 914 (2001) 315-324. DOI: 10.1016/S0021-9673(00)01015-3

[62] B. Chankvetadze, K. Lomsadze, D. Bergenthal, J. Breitkreutz, K. Bergander, G. Blaschke, Mechanistic study on the opposite migration order of clenbuterol enantiomers in capillary electrophoresis with β-cyclodextrin and single-isomer heptakis(2,3-diacetyl-6-sulfo)-β-cyclodextrin, Electrophoresis 22 (2001) 3178-3184. DOI: 10.1002/1522-2683(200109)22:15<3178::AID-ELPS3178>3.0.CO;2-F.

[63] B. Chankvetadze, K. Lomsadze, N. Burjanadze, J. Breitkreutz, G. Pintore, M. Chessa, D. Bergenthal, K. Bergander, G. Blaschke, Comparative enantioseparations with

native β-cyclodextrin, randomly acetylated β-cyclodextrin and heptakis-(2,3-di-O-acetyl)-β-cyclodextrin in capillary electrophoresis, Electrophoresis 24 (2003) 1083-1091. DOI: 10.1002/elps.200390126.

[64] C. Kahle, U. Holzgrabe, G.K.E. Scriba, Studies on the chiral recognition of peptide enantiomers by neutral and sulfated β-cyclodextrin and heptakis-(2,3-di-O-acetyl)β-cyclodextrin using capillary electrophoresis and nuclear magnetic resonance, Electrophoresis 23 (2002) 1301-1307. DOI: 10.1002/1522-2683(200205)23:9<1301::AID-ELPS1301>3.0.CO;2-7

[65] B. Chankvetadze, N. Burjanadze, D. M. Maynard, K. Bergander, D. Bergenthal, G. Blaschke, Comparative enantioseparations with native β-cyclodextrin and heptakis-(2-O-methyl-3,6-di-O-sulfo)-β-cyclodextrin in capillary electrophoresis, Electrophoresis, 2002, 23, 3027-3034. ~~HDMS-b-CD-2001~~, DOI: 10.1002/1522-2683(200209)23:17<3027:AID-ELPS3027>3.0.CO;2-V.

[66] A. Gogolashvili, E. Tatunashvili, L. Chankvetadze, T. Sohajda, J. Szemann, A. Salgado, B. Chankvetadze, Separation of enilconazole enantiomers in capillary electrophoresis with cyclodextrin-type chiral selectors and investigation of structure of selector-selectand complexes by using nuclear magnetic resonance spectroscopy, Electrophoresis 38 (2017) 1851-1859. DOI: 10.1002/elps.201700078.

[67] A. Gogolashvili, E. Tatunashvili, L. Chankvetadze, T. Sohajda, J. Szemann, M. Gumustas, S. Ozkan, A. Salgado, B. Chankvetadze, Separation of terbutaline enantiomers in capillary electrophoresis with cyclodextrin-type chiral selectors and investigation of structure of selector-selectand complexes by using nuclear-magnetic resonance spectroscopy, J. Chromatogr. A, 1571 (2018) 231-239. DOI: 10.1016/j.chroma.2018.08.012.

[68] W.-S. Li, S.-C. Wang, T.-S. Hwang, I. Chao, Substituent effect on the structural behaviour of modified cyclodextrin: a molecular dynamic study on methylated β-CDs, J. Phys. Chem. B 116 (2012) 3477-3489. DOI: 10.1021/jp207985q.

[69] J.F. DeBernardis, D.J. Kerkman, D.L. Arendsen, S.A. Buckner, J.J. Kyncl, A.A. Hancock, Conformationally defined adrenergic agents. 5. Resolution, absolute configuration, and pharmacological characterization of the enantiomers of 2-(5,6-dihydroxy-l,2,3,4-tetrahydro-l-naphthyl)imidazoline: A potent agonist at α-adrenoceptors, J. Med. Chem. 30 (1987) 1011-1017. DOI: 10.1021/jm00389a009.

Figure legends:

Fig. 1 Structure of THZ and schematic representation of CDs under this study.

Fig. 2 CE separation of THZ enantiomers (R/S = 2/1) with various CDs. For experimental conditions see subsection 2.3.

Fig. 3 ^{13}C-NMR spectra of pure (-)-THZ (a) and (-)-THZ mixed with α-CD (b), β-CD (c) and HDAS-β-CD (d). Some regions bearing cyclodextrin signals have been cut for convenience.

Fig. 4 ^{1}H NMR spectrum and selected 1D ROESY traces of THZ : α-CD mixture. For experimental conditions see subsection 2.4.

Fig. 5 Structures of THZ : α-CD (a), THZ : β-CD (b) and THZ : HDAS-β-CD complexes (c) as deduced from ROESY experiments.

Fig. 6 ^{1}H NMR spectrum and selected 1D ROESY traces of THZ : β-CD mixture. For experimental conditions see subsection 2.4.

Fig. 7 ^{1}H NMR spectrum and selected 1D ROESY traces of THZ : HDAS-β-CD mixture. For experimental conditions see subsection 2.4.

Fig. 8 Comparison between V_S (kcal/mol) of β-CD, HDAS- and HMDS-β-CD (HF/STO-3G).

Fig. 9 Structures of THZ : CD complexes calculated with the MMFF94s force field.

a)

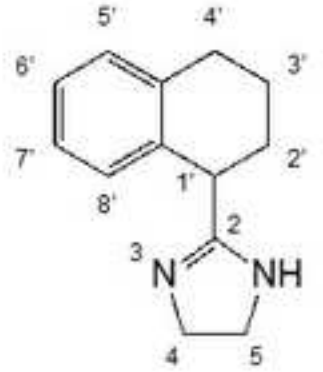

b)

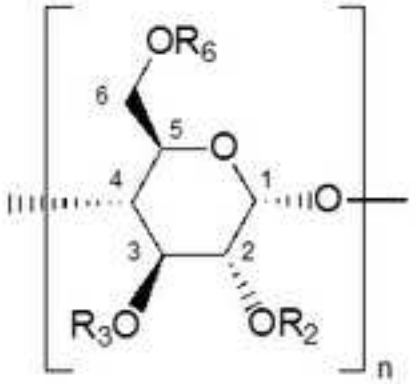

CD	n	Substituent		
		R_2	R_3	R_6
α-CD	6	H	H	H
β-CD	7	H	H	H
γ-CD	8	H	H	H
H-2,3-DM-β-CD	7	CH_3	CH_3	H
H-2,6-DM-β-CD	7	CH_3	H	CH_3
TM-β-CD	7	CH_3	CH_3	CH_3
HDA-β-CD	7	$COCH_3$	$COCH_3$	H
HS-β-CD	7	H	H	SO_3^-
HDMS-β-CD	7	CH_3	CH_3	SO_3^-
HDAS-β-CD	7	$COCH_3$	$COCH_3$	SO_3^-
HMDS-β-CD	7	CH_3	SO_3^-	SO_3^-

Fig. 1

Figure 2

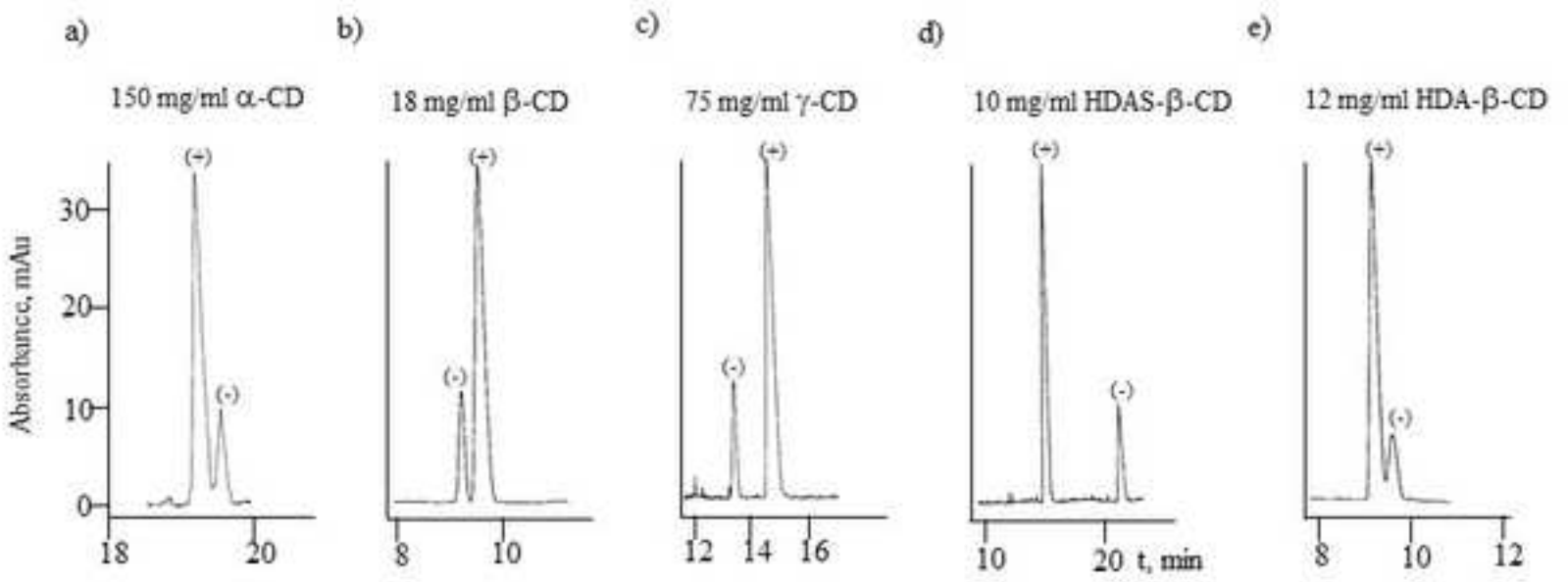

Fig. 2

Figure 3

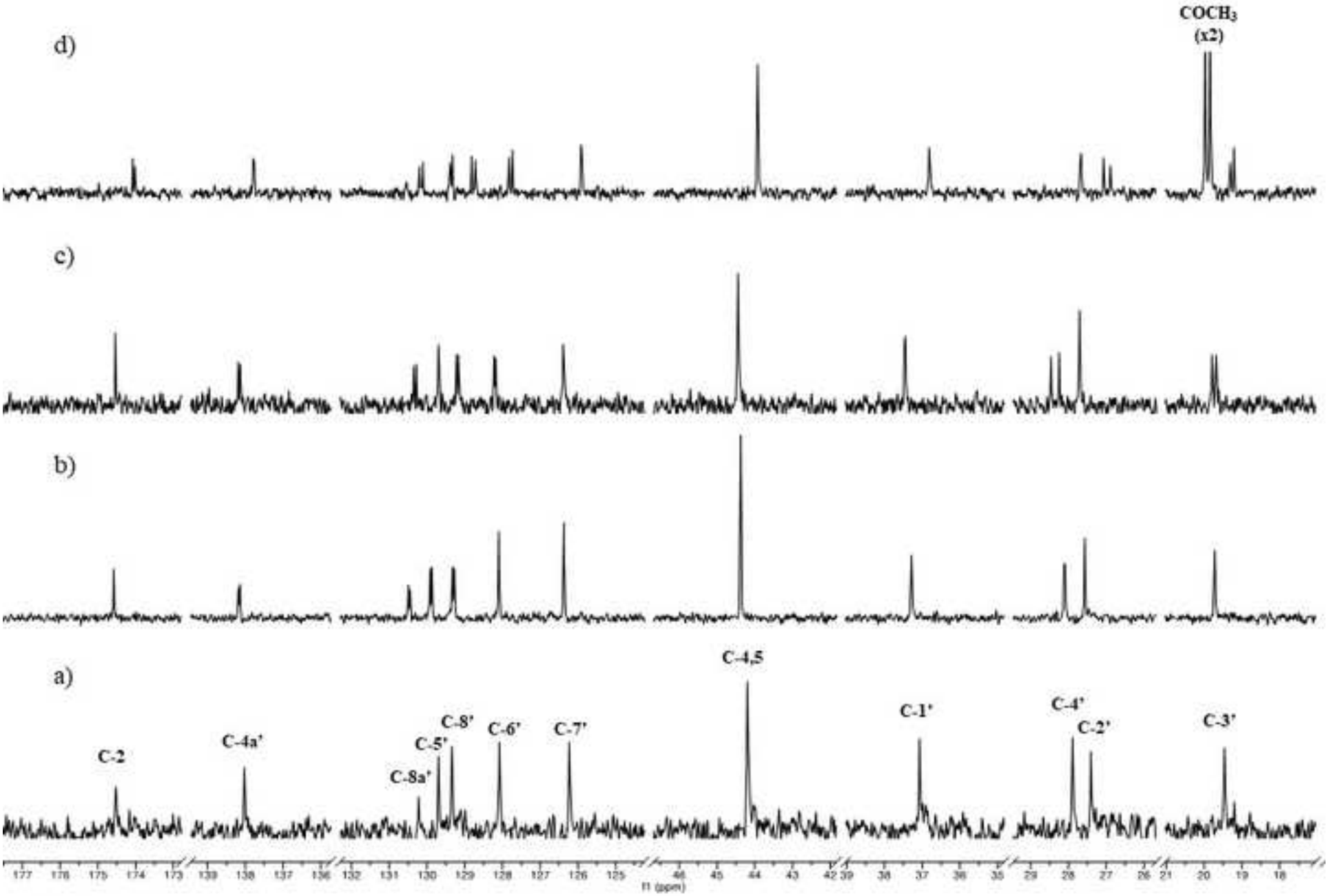

Fig. 3

Figure 4

Click here to access/download;Figure;Slide4.JPG

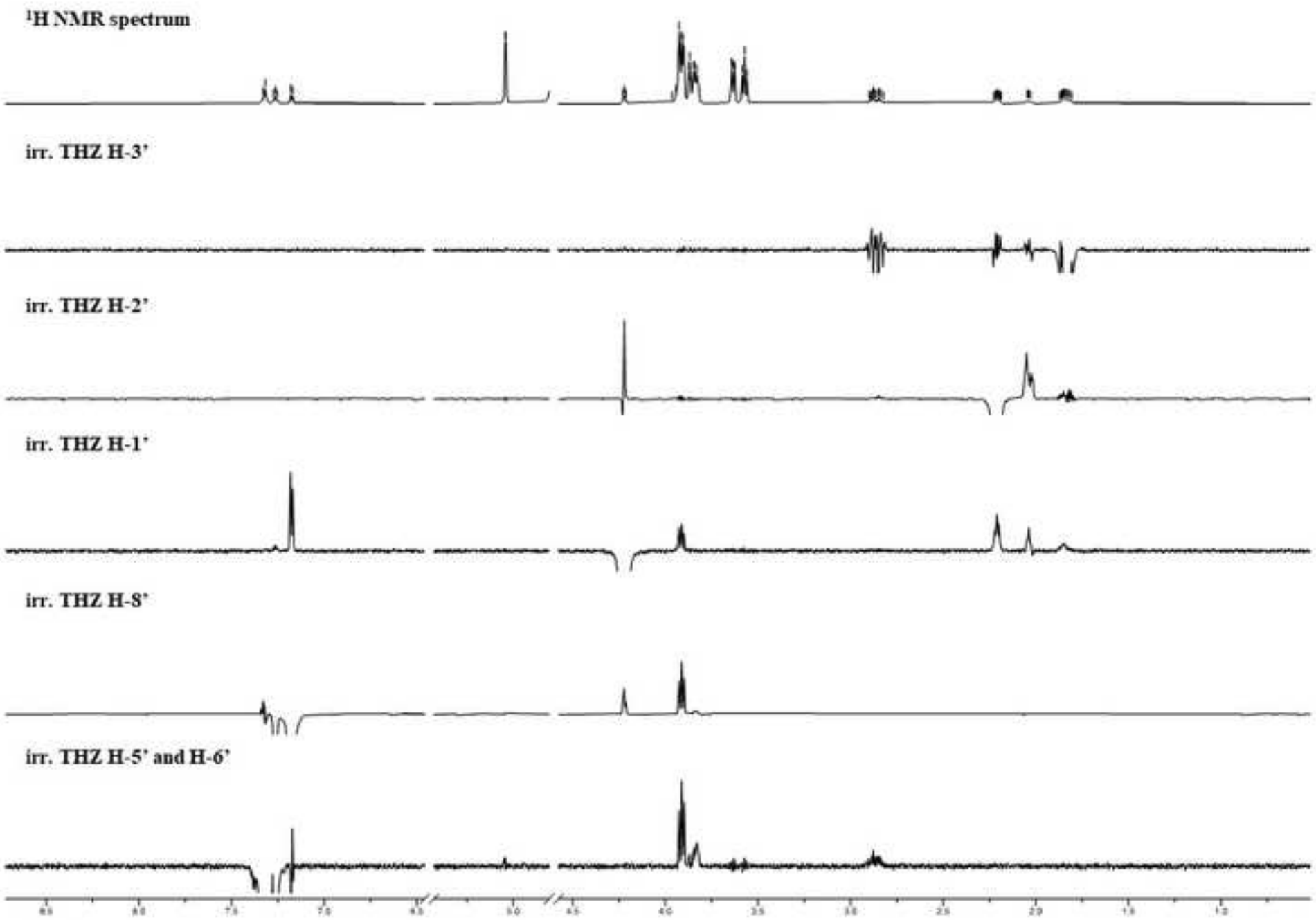

Fig. 4

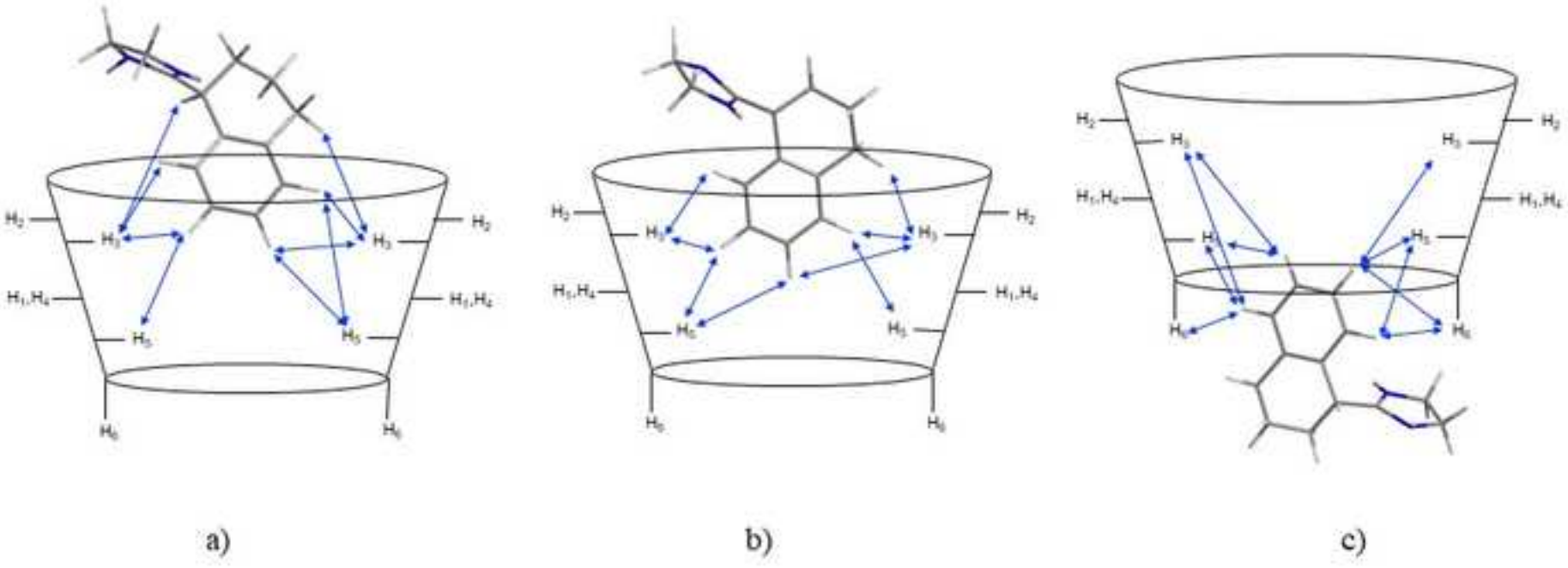

Fig. 5

Figure 6

Click here to access/download;Figure;Slide6.JPG

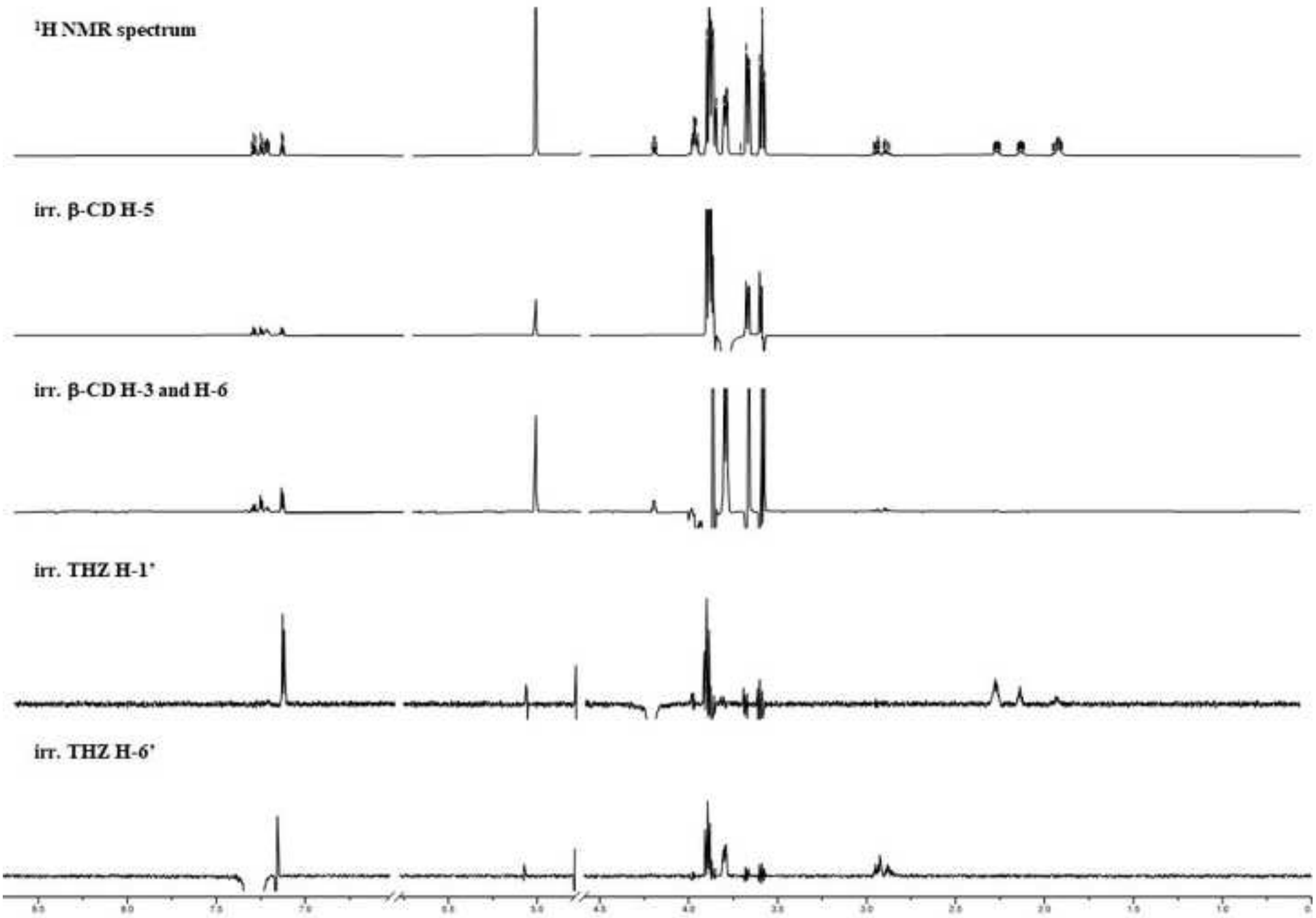

Fig. 6

Figure 7

Click here to access/download;Figure;Slide7.JPG

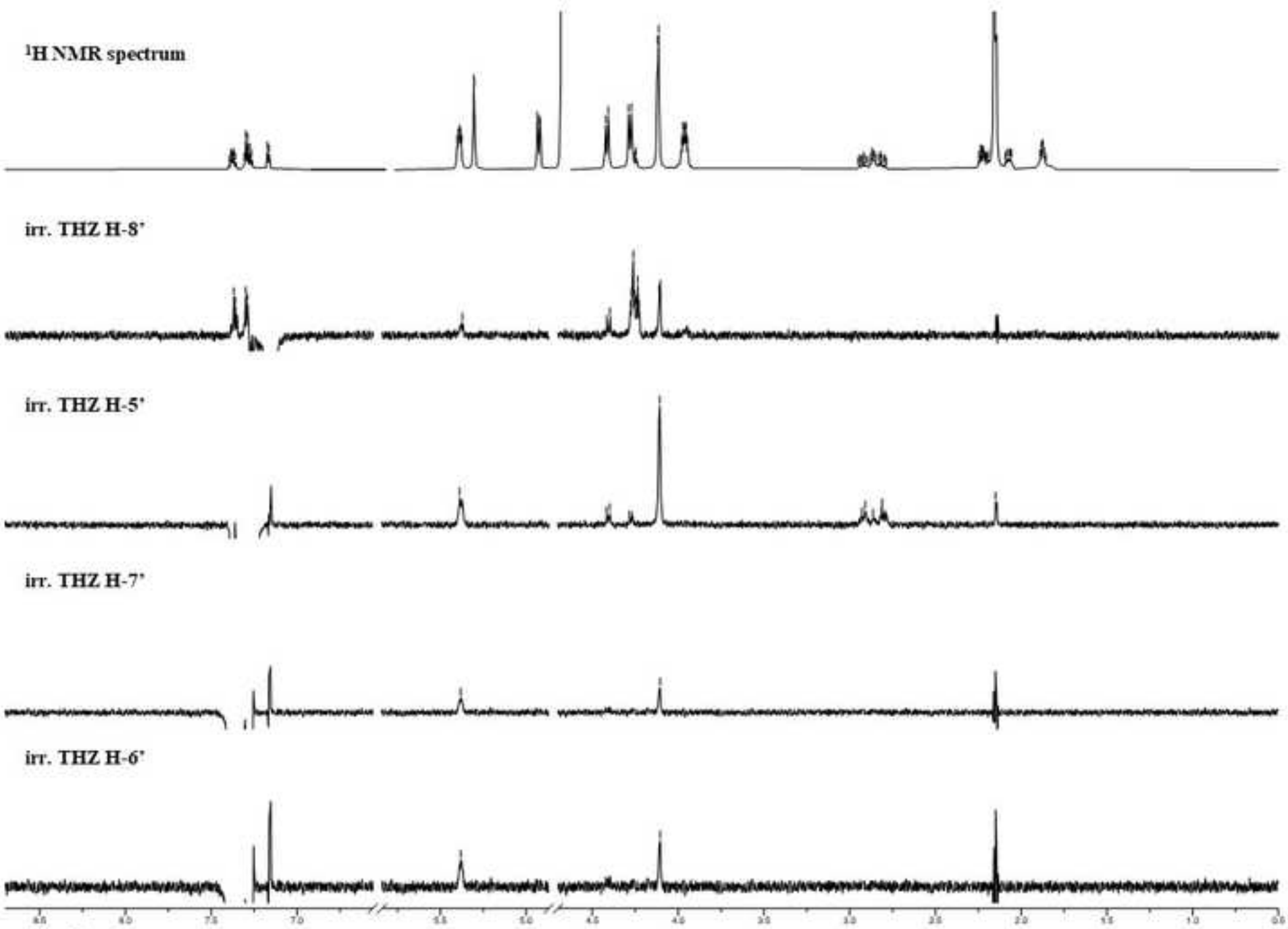

Fig. 7

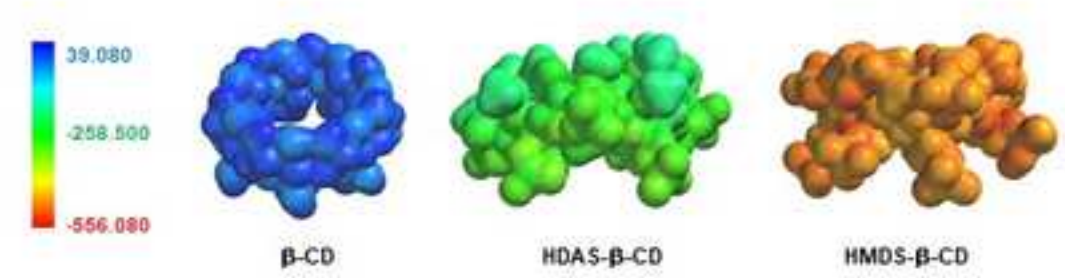

Fig. 8

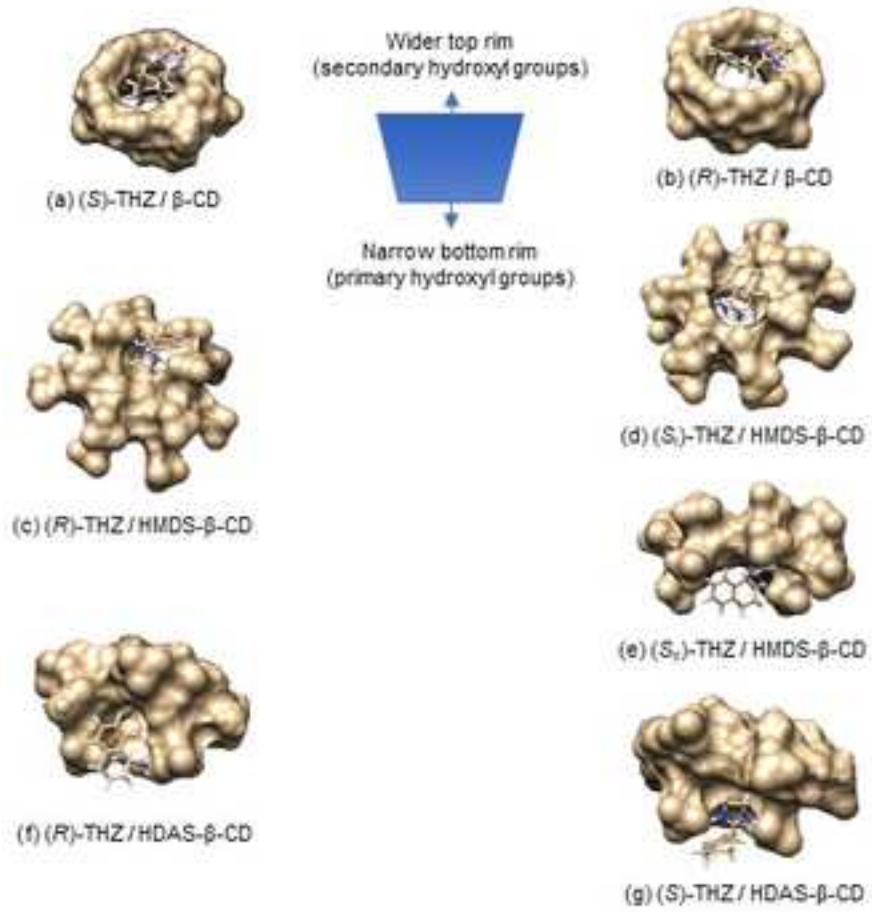

Fig. 9

Table 1 Separation of tetrahydrozoline enantiomers (1/2 mixture) with various cyclodextrins

Cyclodextrin	Concentration, mg/ml	t_1, min	t_2, min	α	Migration order
α-CD	150	18.89	19.34	1.02	+/-
β-CD	18	9.22	9.63	1.04	-/+
γ-CD	75	13.40	14.75	1.10	-/+
H-2,3-DM-β-CD	100	33.40	34.70	1.04	-/+
H-2,6-DM-β-CD	50	14.14	14.48	1.02	-/+
H-TM-β-CD	150	11.99	12.44	1.03	-/+
HDA-β-CD	12	9.54	9.96	1.04	+/-
HS-β-CD	50	17.93	18.72	1.04	-/+
HDMS-β-CD	50	9.31	9.38	1.01	-/+
HDAS-β-CD	10	14.99	20.63	1.38	+/-
HMDS-β-CD	30	7.12	7.52	1.06	+/-

Table 2

^{1}H signal assignments (ppm) in the (-)-THZ complexes with α-CD, β-CD and HDAS-β-CD.

Position	**Complex**		
	(-)-THZ/α-CD	**(-)-THZ/β-CD**	**(-)-THZ/HDAS-β-CD**
(-)-THZ*			
H-4 **H-5**	~3.92 (x4)	~3.98 (x4)	~3.96 (x4)
H-1'	4.22	4.21	4.25
H-2´	2.04, 2.20	2.10, 2.24	2.87 (x2)
H-3'	1.84 (x2)	1.88 (x2)	1.87 (x2)
H-4'	2.86 (x2)	2.88, 2.93	2.07, 2.22
H-5'	7.31	7.28	7.27
H-6'	7.33	7.33	7.37
H-7'	7.29	7.25	7.29
H-8'	7.16	7.16	7.16
CD			
H-1	5.04	5.07	5.30
H-2	3.63	3.67	4.92
H-3	3.93	3.89	5.39
H-4	3.57	3.59	4.11
H-5	3.83	3.78	4.11
H-6	3.86, 3.91	3.86, 3.90	4.28, 4.41
2-OAc	-	-	2.14, 2.15
3-OAc	-	-	

* most signals are doubled due to racemization of (-)-THZ.

Table 3
Binding energies of the THZ / CD complexes (CD = β-CD, HDAS- and HMDS-β-CD) calculated in vacuum (v) and water (w) (SM5.4 model) with the MMFF94s force field.

Entry	CD	Medium	THZ	Energy [kcal/mol]		Enantiomer Migration Order (EMO)	
				$E_{binding}$	$\Delta E_{binding}$[a]	calculated	experimental
1	β	v	*R*	-39.56	4.59	(*S*) > (*R*)	(-) > (+)
2			*S*	-34.97			
3		w	*R*	-24.75	6.09	(*S*) > (*R*)	(-) > (+)
4			*S*	-18.66			
5	HMDS	v	*R*	-620.21			
6			S_I[b]	-625.11	-4.9 (S_I)	(*R*) > (*S*)	(+) > (-)
7			S_{II}[b]	-625.26	-5.05 (S_{II})		
8		w	*R*	-86.44			
9			S_I[b]	-90.03	-3.59 (S_I)	(*R*) > (*S*)	(+) > (-)
10			S_{II}[b]	-104.84	-18.4 (S_{II})		
11	HDAS	v	*R*	-334.82	-15.54	(*R*) > (*S*)	(+) > (-)
12			*S*	-350.36			
13		w	*R*	-33.40	-2.91	(*R*) > (*S*)	(+) > (-)
14			*S*	-36.31			

[a] $\Delta E_{binding} = E_{binding(S)} - E_{binding(R)}$

[b] S_I: (*S*)-THZ located at the wider secondary rim of the HMDS-β-CD; S_{II}: (*S*)-THZ located at the narrow primary rim of the HMDS-β-CD.

Credit Author Statement

Author	Credit/contribution
Ann Gogolashvili	CE experimental work
Ketevan Lomsadze	CE experimental work, Editing
Lali Chankvetadze	CE experimental work, Editing
Nino Takaishvili	CE experimental work
Paola Peluso	Molecular Modeling Calculations, Editing
Roberto Dallocchio	Molecular Modeling Calculations
Antonio Salgado	NMR Experiment, Editing
Bezhan Chankvetadze	Conceptualization, Writing & Editing

Declaration of interests

xThe authors declare that they have no known competing financial interests or personal relationships that could have appeared to influence the work reported in this paper.

☐The authors declare the following financial interests/personal relationships which may be considered as potential competing interests:

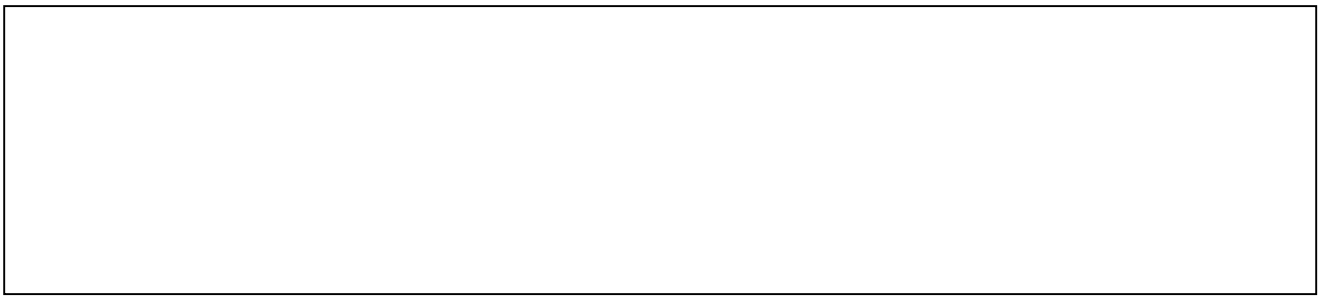

February 10th, 2021.